INTENSITY INHOMOGENEITY CORRECTION OF MACULAR OCT USING N3 AND RETINAL FLATSPACE

Andrew Lang[1], *Aaron Carass*[1], *Bruno M. Jedynak*[2], *Sharon D. Solomon*[3], *Peter A. Calabresi*[4], *and Jerry L. Prince*[1]
[1]Dept. of Electrical and Computer Engineering, The Johns Hopkins University, Baltimore, MD
[2]Dept. of Mathematics and Statistics, Portland State University, Portland, OR
[3]Dept. of Ophthalmology, The Johns Hopkins Hospital, Baltimore, MD
[4]Dept. of Neurology, The Johns Hopkins Hospital, Baltimore, MD

ABSTRACT

As optical coherence tomography (OCT) has increasingly become a standard modality for imaging the retina, automated algorithms for processing OCT data have become necessary to do large scale studies looking for changes in specific layers. To provide accurate results, many of these algorithms rely on the consistency of layer intensities within a scan. Unfortunately, OCT data often exhibits inhomogeneity in a given layer's intensities, both within and between images. This problem negatively affects the performance of segmentation algorithms and little prior work has been done to correct this data. In this work, we adapt the N3 framework for intensity inhomogeneity correction, which was originally developed to correct MRI data, to work for macular OCT data. We first transform the data to a flattened macular space to create a template intensity profile for each layer giving us an accurate initial estimate of the gain field. N3 will then produce a smoothly varying field to correct the data. We show that our method is able to both accurately recover synthetically generated gain fields and improves the stability of the layer intensities.

Index Terms— OCT, inhomogeneity correction, flat space, retina

1. INTRODUCTION

Optical coherence tomography (OCT) has become a standard clinical modality for imaging the eye, rapidly providing three-dimensional, high resolution images of the retina, a structure vital to healthy vision. The retina comprises several layers, and by measuring the thickness of these layers, we are able to assess the health of the eye. Specifically, individual layers may thicken or thin over the course of different diseases, with the amount of change often correlated to disease status or progression.

To make large scale studies of different diseases and their effects on the retina feasible, automated algorithms have been developed to segment layers and measure their thickness [1, 2]. Many of these algorithms rely on having consistent intensities within each layer to perform well. Among the many types of artifacts found in OCT data, intensity inhomogeneity is one which can significantly impact the accuracy of layer segmentation [3]. Inhomogeneity in OCT data often appears in images with poor scan quality, off center acquisitions, and after multi-frame averaging, and may be caused by problems including opacity of transparent ocular media (e.g. cataracts) and vignetting due to misalignment, among other things. As a result, both normalization of the intensities and correction of inhomogeneity are important to improve image consistency and potentially algorithm performance.

Little prior work has been done to correct for intensity inhomogeneity in retinal OCT images, particularly as a pre-processing step before segmentation. Intensity normalization, where a simple scale factor is used to rescale the intensities to lie within a fixed range, has been applied, but this normalization fails to correct for inhomogeneity within an image [1, 2]. Kraus et al. [4] included illumination correction for motion correction whereby intensities were corrected based on the fundus projection image. There is no correction in depth, however, which may be necessary. Recently, Chen et al. [5] used histogram matching to normalize intensities between scans, which requires careful selection of the reference histogram. Finally, we note that depth-based attenuation correction such as that of Girard et al. [6] can be thought of as a means to correct inhomogeneity in the data, but the contrast of the image is altered and smoothness between A-scans is not enforced.

One objective of inhomogeneity correction in OCT data is to equalize the intensities within each layer. Since this is intended to be a pre-processing step, a layer segmentation is not available, so the normalization must be constructed in a more structured way. With this in mind, we adapt the non-parametric nonuniform intensity normalization (N3) method to work for OCT data [7]. N3 is a standard method for inhomogeneity correction of brain MRI data. Direct application of N3 to OCT corrects for large inhomogeneity artifacts, but

This work was supported by the NIH/NEI through grant R01-EY024655.

fails to equalize the intensities within each layer. To improve the performance, we first convert the data to a macular flat space (MFS), which transforms the data such that the layers are approximately flat. This transformation allows us to accurately initialize the algorithm to have better convergence to the desired solution. It also allows regularization within each layer to maintain consistency.

2. METHODS

Our inhomogeneity correction algorithm follows two main steps. First, we convert the data to the MFS. To do this, we use an estimate of the inner and outer boundaries of the retina, which are found as described in our previous work [2]. Second, with the data in the MFS, we are able to directly run the N3 algorithm. Together, we refer to this as the N3 for OCT (N3O) method.

2.1. Macular Flat Space (MFS)

To build the MFS, we use a regression model to estimate the boundary positions of each layer given an initial segmentation of the inner and outer retinal boundaries. Using the output of this model, we deform the data such that each regression boundary is flat. As Fig. 1 shows, the layers in the deformed data are generally flat across the image, despite any errors in the estimated boundaries.

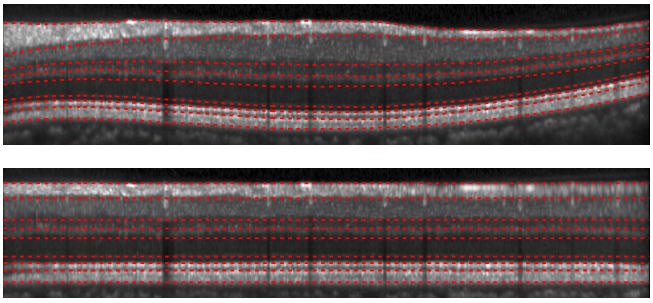

Fig. 1. A B-scan image with regression estimated boundaries overlaid in the native (top) and macular flat space (bottom).

Construction of the MFS follows from our previous work [8, 9] with three important differences: the use of a quadratic regression model instead of a linear one, added spatial regularization to improve the stability of the regression fit, and added smoothness to the deformation field to remove discontinuity artifacts produced by the transformation. Given initial segmentations of the inner and outer retinal boundaries, $b_1(x)$ and $b_2(x)$, and the thickness between them, $t(x) = b_2(x) - b_1(x)$, the regression boundaries, $r_i(x)$, are estimated from their distance to the top boundary using the equation

$$r_i(x) = b_1(x) + \alpha_{i,1}(x) + \alpha_{i,2}(x)t(x) + \alpha_{i,3}(x)t(x)^2 \quad (1)$$

where $\alpha_{i,j}(x)$ are the regression coefficients to be estimated for boundary i at A-scan location x. Given an $L \times M \times N$ volume, there are MN A-scans and $3MN$ coefficients to estimate for each boundary. To find these coefficients, we solve the minimization problem

$$\arg\min_{\boldsymbol{\alpha}_i} \|\mathrm{A}\boldsymbol{\alpha}_i - \mathbf{r}_i\|^2 + \lambda \|\Gamma\boldsymbol{\alpha}_i\|^2 \quad (2)$$

where A is a block diagonal matrix, Γ penalizes the difference in coefficient values between adjacent A-scans, and λ is a weight which balances the smoothness of the solution. Note that both A and Γ are large, sparse matrices, which allows the problem to be efficiently solved using QR decomposition.

The values of $\mathbf{r}_i$ used to solve (2) are from manual segmentations of OCT data for 37 subjects. Nine boundaries on all B-scans were delineated for each subject. Scans from different subjects were aligned by translating the data to align the center of the fovea, which is taken as the shortest distance between $b_1(x)$ and $b_2(x)$.

To convert the data to the MFS, we create a 3-dimensional deformation field where vertical displacement vectors are placed on the regression boundaries in each A-scan such that the resulting deformed boundaries are flat, and the distance between adjacent flat boundaries equals the average thickness of the respective layer over the volume. The resulting set of boundary displacements are then interpolated between the boundaries in each A-scan using a cubic Hermite spline to ensure the displacements are both smooth and monotonic.

2.2. Intensity normalization

We normalize the intensities of the data following the N3 algorithm [7]. We briefly describe the algorithm here, with more specific details found in [7]. A multiplicative model of the data is assumed with the intensity at position $\mathbf{x}$ given by $v(\mathbf{x}) = u(\mathbf{x})f(\mathbf{x}) + n(\mathbf{x})$, where u is the true image, f is a smoothly varying gain field, and n is normally distributed noise. An additive model for the gain field is created by taking the logarithm of the data: $\log v(\mathbf{x}) = \hat{v}(\mathbf{x}) = \hat{u}(\mathbf{x}) + \hat{f}(\mathbf{x})$. The additive field $\hat{f}$ is assumed to be smoothly varying with intensity distribution $\mathcal{N}(0, \sigma)$. At each iteration of the algorithm, $\hat{u}$ is estimated using $\hat{f}$ at the previous iteration and then sharpened using the assumed normal distribution of $\hat{f}$. The resulting field estimate from the sharpened $\hat{u}$ is then smoothed using a cubic B-spline. These steps are iterated until the field estimate converges to within a given threshold.

For smoothing of the gain field at each iteration, we follow the efficient P-spline framework of Eilers et al. [10]. Smoothness is controlled by two factors: the spacing of the B-spline control points over the data, and the weight of the regularization term enforcing smoothness between the B-spline coefficients, where we use second order differences.

To improve the convergence of the algorithm, we use an initial estimate of the gain field instead of initializing with zeros. Since the data is in MFS, all pixels on the same horizontal

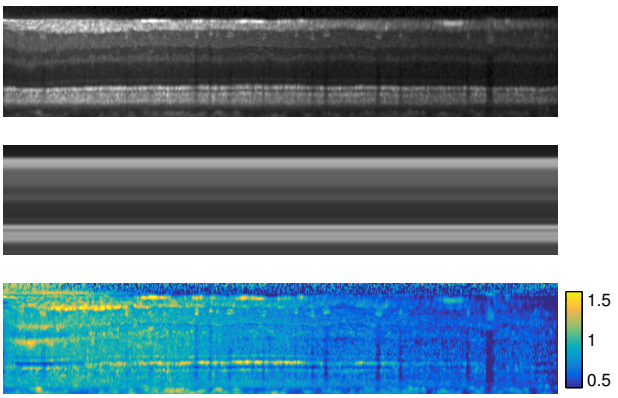

Fig. 2. The initial gain field (bottom) is generated by dividing the flat space data (top) by the averaged template image (middle).

plane are assumed to lie in the same layer. We build a template A-scan intensity profile by averaging the flat space data horizontally across all A-scans and B-scans. A full template volume is then found by replicating this profile to the size of the data. In Fig. 2, we show a flat space B-scan, the template B-scan, and the initial gain field found as the ratio of the two images. Note that we cannot use this field directly to normalize the data due to misalignment of the flatspace boundaries.

The final normalized image is computed after inverting the flatspace transformation on the gain field. Since the MFS crops out the background region, we linearly extrapolate the gain field on the boundaries to have a value of 1 away from the retinal area.

3. EXPERIMENTS AND RESULTS

We evaluated our method using OCT data acquired from a Heidelberg Spectralis scanner (Heidelberg Engineering, Heidelberg, Germany). Volumetric scans from 41 subjects were acquired having 496 pixels per A-scan, 1024 A-scans per B-scan, 49 B-scans per volume.

The algorithm has several parameters which need to be specified. Parameters of N3 not mentioned here were left at the default values. We used control point spacing of 80 μm vertically and 500 μm horizontally. The regularization weight was set to 10. These provided good results, but a more rigorous treatment to find the best values will be necessary. A value of $\lambda = 0.5$ was used for the MFS regression, but the transformation is quite robust to the exact value used.

3.1. Synthetic gain field

We begin by evaluating the performance of N3O by assessing how well it recovers an artificially generated gain field applied to a chosen B-scan which is homogeneous in appearance. Two types of artificial fields were produced. The first

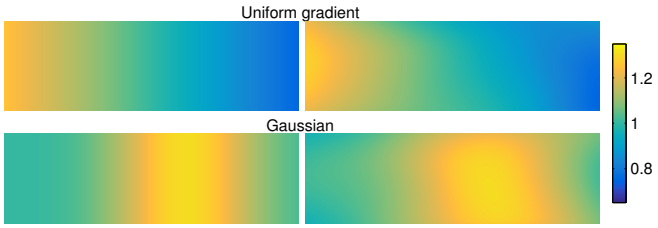

Fig. 3. Examples of synthetic gain fields constructing having a uniform gradient (top) and Gaussian shape (bottom). The true and estimated fields are on the left and right, respectively.

Table 1. Average correlation coefficient between the true synthetic gain field and the initialization and N3O over 100 trials with standard deviation in parentheses.

Uniform initial	Uniform N3O	Gaussian initial	Gaussian N3O
0.54 (0.21)	0.98 (0.02)	0.43 (0.16)	0.90 (0.09)

was randomly generated having a constant gradient horizontally across the image, with a random magnitude between 10% and 50% of the maximum intensity of the data. The second field type was produced having a Gaussian shape with magnitude again between 10% and 50%, standard deviation between 0.25 and 1.25 mm, and centered at a random A-scan. An example of each field is shown in Fig. 3 along with the N3O estimated result.

We use the correlation coefficient to compare the result of N3O with the true field. One hundred randomly generated fields of each type were used to evaluate the algorithm with the results in Table 1. To provide a reference, we also include the correlation coefficients for the initial field produced from the template B-scan (e.g. like in Fig. 2). Note that the N3O result was significantly better than the initialization in both cases ($p < 0.0001$).

3.2. Intensity variability

Next, we look at the average standard deviation of the intensities within each layer across all subjects. Layers were defined based on the manual segmentation of the boundaries by a single trained rater for all 41 scans. We compared N3O results with no correction, and with the use of an intensity normalization which rescales the intensity of each B-scan to a robust estimate of the maximum intensity [2]. Fig. 4 shows a plot of the results. The new method has significantly less variability in all layers when compared to either the original and normalized data ($p < 0.0001$ using a two-sided Student's t-test).

3.3. Qualitative assessment

Finally, we present a qualitative assessment of N3O. Figure 5 shows an input image, the corrected image, and the estimated gain field for two B-scans from two different subjects. While

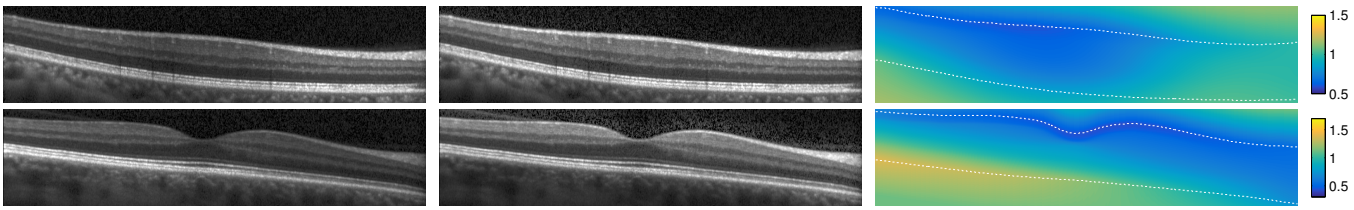

Fig. 5. Input images from two different subjects (left) before, (middle) after, and (right) the resulting gain field.

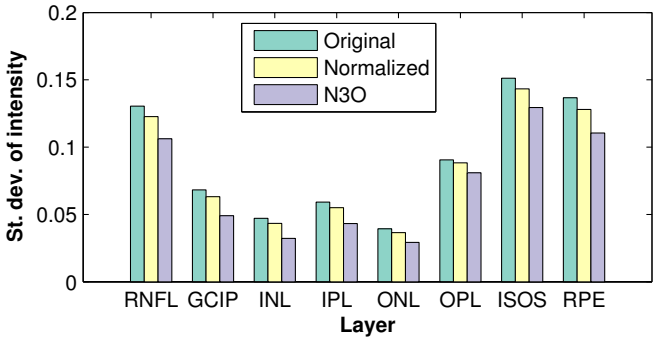

Fig. 4. Bar plot of the standard deviation of the intensities within each layer averaged across all subjects.

the images exhibit different inhomogeneity patterns, the algorithm is able to correct both images. We see that the gain patterns vary slowly, which is a result of the regularization enforced by the spline fit. We also see the potentially adverse affect of using a multiplicative gain field model by the amplified noise intensity in darker regions.

4. CONCLUSIONS

We have adapted a previously described method of intensity inhomogeneity correction to work for OCT data. One important addition included for the processing of OCT was the use of the MFS, the importance of which is twofold. First, we are able to create an accurate initial estimate of the gain field, improving the convergence of the algorithm. Second, since the smoothness of the field is enforced along rows and columns by regularization, the gain field varies smoothly within the flattened layers. This is desirable since the corrected intensities should be uniform within a layer.

In the future, we will look to evaluate the effect of N3O on the performance of automated layer segmentation algorithms. Since many of these algorithms do not currently incorporate this type of pre-processing, we expect N3O to improve both their stability and accuracy. We have presented the first step in what will be a larger evaluation into the effects of inhomogeneity correction, as well as intensity normalization. Inhomogeneity correction has become ubiquitous and essential for the processing of data in other applications including brain MRI and could prove to be equally important for OCT. We hope to explore this idea going forward, along with a thorough evaluation of the algorithm parameters to come up with a standard in the same way N3 is used.

5. REFERENCES

[1] I. Ghorbel et al., "Automated segmentation of macular layers in OCT images and quantitative evaluation of performances," *Pattern Recognition*, vol. 44, no. 8, pp. 1590–1603, 2011.

[2] A. Lang et al., "Retinal layer segmentation of macular OCT images using boundary classification," *Biomed. Opt. Express*, vol. 4, no. 7, pp. 1133–1152, 2013.

[3] I. C. Han et al., "Evaluation of artifacts associated with macular spectral-domain optical coherence tomography," *Ophthalmology*, vol. 117, no. 6, pp. 1177 – 1189.e4, 2010.

[4] M. F. Kraus et al., "Quantitative 3D-OCT motion correction with tilt and illumination correction, robust similarity measure and regularization," *Biomed. Opt. Express*, vol. 5, no. 8, pp. 2591–2613, 2014.

[5] C.-L. Chen et al., "Histogram matching extends acceptable signal strength range on optical coherence tomography images histogram matching extends OCT data usability," *Invest. Ophthalmol. Vis. Sci.*, vol. 56, no. 6, pp. 3810, 2015.

[6] M. J. A. Girard et al., "Shadow removal and contrast enhancement in optical coherence tomography images of the human optic nerve head," *Invest. Ophthalmol. Vis. Sci.*, vol. 52, no. 10, pp. 7738, 2011.

[7] J. G. Sled et al., "A nonparametric method for automatic correction of intensity nonuniformity in MRI data," *IEEE Trans. Med. Imag.*, vol. 17, no. 1, pp. 87–97, 1998.

[8] A. Lang et al., "An adaptive grid for graph-based segmentation in retinal OCT," *Proc. SPIE*, vol. 9034, pp. 903402, 2014.

[9] A. Carass et al., "Multiple-object geometric deformable model for segmentation of macular OCT," *Biomed. Opt. Express*, vol. 5, no. 4, pp. 1062–1074, 2014.

[10] P. H. C. Eilers et al., "Fast and compact smoothing on large multidimensional grids," *Comput. Stat. Data Anal.*, vol. 50, no. 1, pp. 61 – 76, 2006.